

EA-BEV: Edge-aware Bird's-Eye-View Projector for 3D Object Detection

Haotian Hu

hht1996ok@zju.edu.cn

Fanyi Wang

11730038@zju.edu.cn

Jingwen Su

j_su95@outlook.com

Laifeng Hu

hlf@alu.uestc.edu.cn

Tianpeng Feng

tianpeng_feng@whu.edu.cn

Zhaokai Zhang

zhangzhaokai1@oppo.com

Wangzhi Zhang*

zhiwang.zhang@sydney.edu.au

Abstract

In recent years, significant progress has been made in Lift-Splat-Shot-based (LSS-based) 3D object detection methods, which transform features from 2D camera views and 3D LiDAR views into a Bird's-Eye-View (BEV) for feature fusion. However, inaccurate depth estimation, such as the "depth jump" problem, remains a challenge for further development of LSS-based techniques. To mitigate the "depth jump" issue, we propose an Edge-Aware Bird's-Eye-View (EA-BEV) projector. By integrating the proposed edge-aware depth fusion module with the depth estimation module, our EA-BEV projector addresses this problem while providing refined depth supervision. Additionally, we introduce sparse depth supervision and gradient edge depth supervision to constrain learning on global depth and local marginal depth information. Our EA-BEV projector serves as a plug-and-play module for any LSS-based 3D object detection model, effectively enhancing baseline performance. We demonstrate the effectiveness of our approach on the nuScenes benchmark. On the nuScenes 3D object detection validation dataset, our proposed EA-BEV projector significantly improves several state-of-the-art LSS-based baselines on the nuScenes 3D object detection benchmark and nuScenes BEV map segmentation benchmark, with only a negligible increase in inference time. Code to reproduce our results is available at <https://github.com/hht1996ok/EA-BEV>.

1. Introduction

As the complexity of autonomous driving and vehicle sensors continues to increase, it is essential to integrate multiple sources of information (e.g., 2D multi-view images from cameras and point clouds from LiDAR) from various

sensors and generate a unified feature representation.

Projecting different information sources onto a Bird's-Eye-View (BEV) has become a popular trend, garnering significant attention from both academia and industry. One of the core challenges in BEV perception is the reconstruction of lost depth information from 2D images, and providing accurate feature distribution for subsequent network processing.

Lift-Splat-Shot-based (LSS-based) methods [8, 7, 31, 25] predict the depth distribution of each grid on 2D features, and "lift" the 2D features of each grid into voxel space using the predicted depth distribution. However, due to significant depth differences between certain regions in 2D images, the depth estimation module struggles to accurately learn depth distribution, resulting in shifted or lost object edge semantic information in the voxel.

We refer to this issue as the "depth jump" problem. As illustrated in Figure 1 (b), the black vacant areas of foreground vehicle edges in the red box indicate the poor performance of the depth estimation module in previous LSS-based methods (e.g., BEVFusion [31]) when dealing with "depth jump" areas. In contrast, after incorporating the EA-BEV projector, the fitting effect is significantly improved.

Moreover, previous LSS-based methods are unable to fully utilize depth information for supervising depth estimation tasks. For instance, BEVDet [7] does not consider point cloud depth information to constrain the depth estimation module. BEVFusion [31] employs a depth map projected from point clouds to implicitly supervise the depth estimation network, but fails to fully leverage the accurate depth information. BEVDepth [25] utilizes min-pooling and one-hot operations to align the predicted depth map with the projected depth map from the point clouds. However, the projected depth maps become extremely sparse after being projected into 2D, which hinders the network from learning accurate depth estimations.

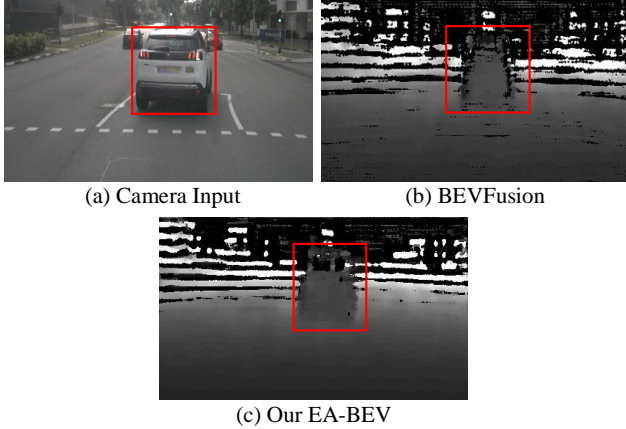


Figure 1. Visualisation of “depth jump” problem. It shows depth estimation before and after adding EA-BEV on baseline method BEVFusion [31]. The larger the pixel value, the deeper the depth.

To alleviate the “depth jump” issue and more effectively leverage depth information for supervising depth prediction tasks, we introduce the Edge-Aware Bird’s-Eye-View (EA-BEV) projector. As depicted in Figure 1 (c), our EA-BEV projector results in more precise depth estimations on the edges of foreground vehicles within the red box. This plug-and-play projector can be seamlessly integrated into any LSS-based method.

Additionally, we present an edge-aware depth fusion module to further mitigate the “depth jump” problem. By incorporating the geometric information of object edges (i.e., prior knowledge), our edge-aware depth fusion module captures fine-grained local edge depth details.

We also suggest gradient edge depth supervision to better accommodate rapid depth changes between objects. To fully harness depth information for supervising depth prediction tasks, we introduce a depth estimation module that incorporates an 8x upsampling operation for sparse depth supervision.

To evaluate the effectiveness and efficiency of our proposed EA-BEV projector, we conduct experiments on the nuScenes dataset [4]. The EA-BEV projector significantly enhances the performance of several state-of-the-art LSS-based baselines [7, 31, 25], while the increase in inference time remains negligible. This leads to state-of-the-art performance on the nuScenes 3D object detection validation set. Furthermore, to assess the generalization capability of our EA-BEV projector, we perform experiments on nuScenes BEV map segmentation benchmarks.

The contributions of this paper are as follows:

- 1) To alleviate the “depth jump” issue and enhance the utilization of depth information for supervising depth prediction tasks, we introduce the Edge-Aware Bird’s-Eye-View (EA-BEV) projector specifically designed for 3D ob-

ject detection tasks.

- 2) We propose an edge-aware depth fusion module and gradient edge depth supervision to mitigate the “depth jump” problem, as well as a depth estimation module to generate a more accurate estimated depth distribution.

- 3) Comprehensive experiments illustrate that our proposed EA-BEV projector significantly improves the performance of several state-of-the-art BEV baselines on the nuScenes 3D object detection benchmark and nuScenes BEV map segmentation benchmark, while incurring only a negligible increase in inference time.

2. Related Work

3D object detection is one of the core tasks of 3D perception, predicting object types and 3D bounding boxes. Previous works [23, 20] directly predict from perspective view (PV) features, which are unable to exploit stereo visual cues from multiple views and time-continuous frames. BEV-based 3D object detection models [31, 10, 2, 7] are beneficial to fuse multi-source and multi-timestamp features, and these models have made great progress in terms of efficiency and performance.

3D object detection is a crucial task in 3D perception, involving the prediction of object types and 3D bounding boxes. Previous works [23, 20] primarily rely on perspective view (PV) features, which do not effectively exploit stereo visual cues from multiple views and time-continuous frames. BEV-based 3D object detection models [31, 10, 2, 7], on the other hand, facilitate the fusion of multi-source and multi-timestamp features, resulting in significant advancements in efficiency and performance.

One of the core problems of BEV perception lies in reconstructing the lost 3D information using PV-to-BEV view translation. To compensate the difference between these two views, previous methods can be divided into network-based view transformation methods [12, 1, 32, 26, 24] and depth-based view transformation methods [7, 2, 28, 15, 21]. They are represented in Section 2.1 and Section 2.2, respectively.

2.1. Network-based View Transformation Methods

2.1.1 MLP-based Approach

MLP-based approaches employ MLP to learn an implicit representation of camera calibration for converting between the two different views. HDMapNet [12] recognizes that one-way projection makes it difficult to ensure effective transfer during the forward pass of view information from PV to BEV, and thus uses an MLP to backward-project features from BEV to PV. VED [1] is the first method to employ end-to-end learning on monocular images for real-time generation of semantic-metric occupancy grid maps. It transforms PV feature maps into BEV feature maps through

flattening, mapping, and reshaping operations for multi-modal perception and prediction.

2.1.2 Transformer-based Approach

Transformer-based approaches directly apply transformers to map PV into BEV, without explicitly requiring the camera model. Tesla first employs a transformer to project PV features into BEV, utilizing positional encoding to design a set of BEV queries and performing view transformations through a cross-attention mechanism between BEV queries and image features. BEVFormer [32] employs deformable attention to extract dense queries in BEV and describe relationships between multi-view features. DETR3D [26] uses a geometry-based feature sampling process instead of cross-attention to predict 3D reference points and projects these reference points onto the 2D image plane using a calibration matrix, enabling end-to-end 3D edge prediction. PETRv2 [24] extends 3D position embedding into the time domain, effectively utilizing continuous frame information. PolarDETR [14] reformulates 3D object detection parameters in the polar coordinate system, revising edge parameterization, network prediction, and loss calculation.

2.2. Depth-based View Transformation

2.2.1 Point-based Approach

Point-based approaches use depth estimation to convert image pixels into pseudo-laser point clouds, and feed to a lidar-based 3D detector. However, these approaches are highly dependent on the accuracy of depth estimation. Pseudo-lidar++ [28] improves the accuracy of depth estimation network using a stereo vision estimation network. SFD [21] uses both the original point cloud and the pseudo point cloud generated by depth estimation network, and fuses them to improve detection accuracy of distant and occluded objects.

2.2.2 Depth Estimation-based Approach

Depth estimation-based methods explicitly predict depth distribution of image features to construct 3D features. These methods are represented by LSS. It predicts both feature distribution in the depth direction and image context information to determine the features of each point of the perspective ray, reducing the loss of image semantics due to depth prediction bias.

BEVDet [7] proposes a multi-view 3D detection framework that includes an image view encoder, view transformer, BEV encoder, and detection head. CaDDN [2] interpolates the sparse depth map into lidar point projection and supervises the depth estimation using depth distribution. MV-FCOS3D++ [15] proposes the pre-training of

depth estimation and monocular 3D detection, which significantly enhances the learning ability of 2D backbones.

Our proposed EA-BEV projector explores the refined depth estimation-based approach by using the proposed depth estimation module and edge-aware depth fusion module. EA-BEV framework is enabled to accurately estimate the global depth and the edge regions of objects with sharp depth changes. And “depth jump” problem is effectively alleviated, which is meaningful to properly guide subsequent network.

3. Method

In Section 3.1, the overview of LSS framework for Bird’s-Eye-View 3D Object Detection is introduced. In Section 3.2, we introduce our proposed EA-BEV Projector that can be used in any LSS-based method. The proposed edge-aware depth fusion module, semantic DepthNet module and depth estimation module are represented in Section 3.3, Section 3.4, and Section 3.5, respectively. Our proposed sparse depth supervision is included in Section 3.5 and gradient depth supervision in 3.6.

3.1. Overview of LSS Framework

In this section, we provide an overview of the LSS framework, as illustrated in Figure 2. The LSS framework employs both 2D input (i.e., 2D multi-view images from a camera) and 3D input (i.e., point clouds from LiDAR) to generate bounding boxes for vehicles, pedestrians, and other objects.

Given the 2D multi-view camera images, a 2D encoder (i.e., Swin-Transformer [11]) extracts 2D camera features. These features, along with the 3D point clouds, are input into our proposed EA-BEV projector to generate frustum features. Following the BEV pooling operation, we obtain the camera BEV feature. LiDAR features are extracted from 3D point clouds using a LiDAR encoder (i.e., SECON [27]).

After obtaining both LiDAR BEV features and camera BEV features, a fusion module and a BEV decoder are employed to generate dense BEV features. With the detection head, bounding boxes for the target objects are produced.

3.2. Edge-aware Bird’s-Eye-View Projector

In this section, we introduce our proposed Edge-aware Bird’s-Eye-View (EA-BEV) projector, which is represented by the orange block in Figure 2. The EA-BEV projector comprises the proposed Edge-aware Depth Fusion module (grey block), Semantic DepthNet Module (yellow block), and Depth Estimation Module (green block).

The inputs of the EA-BEV projector are 2D camera features \mathbf{V}^{cam} and point clouds \mathbf{P} . The point clouds \mathbf{P} are fed into the edge-aware depth fusion module to generate edge-aware depth features \mathbf{F}^{ea} , which are concatenated with 2D

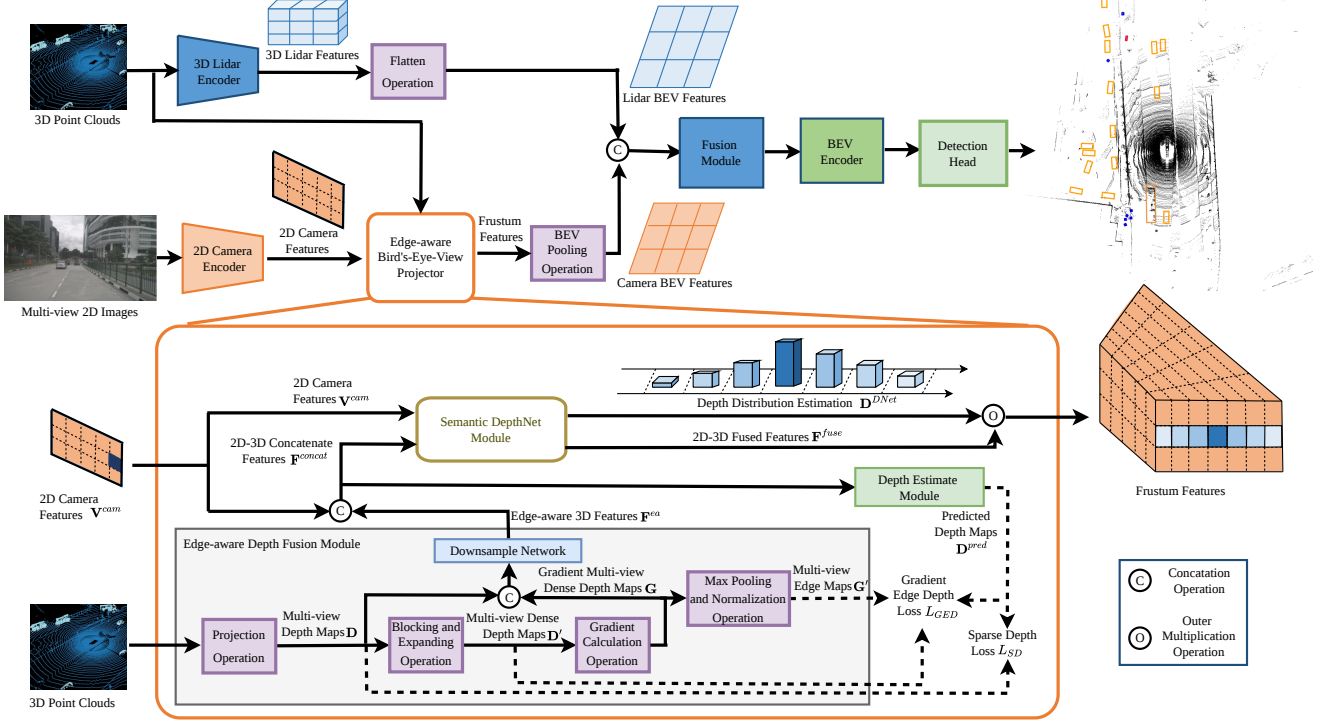


Figure 2. Overview of LSS framework [8] and our proposed EA-BEV projector. LSS framework uses both 2D input (i.e., 2D multi-view images from camera) and 3D input (i.e., point cloud from lidar) to generate bounding boxes of vehicle, pedestrian, etc. Our proposed EA-BEV projector (orange block) contains the proposed Edge-aware Depth Fusion Module (grey block), Semantic DepthNet Module (yellow block), and Depth Estimation Module (green block). Besides, the Sparse Depth Supervision and Gradient Edge Depth Supervision are represented with dotted arrows.

camera features V^{cam} to form 2D-3D concatenated features F^{concat} . Then, predicted depth maps D^{pred} are generated by the depth estimation module.

2D-3D concatenated features F^{concat} , along with 2D camera features V^{cam} , are fed into the Semantic DepthNet module to generate 2D-3D fused features F^{fuse} and predicted depth map D^{DNet} . After the outer multiplication operation, the frustum features are obtained, which is the output of the EA-BEV projector.

3.3. Edge-aware Depth Fusion Module

In this section, we introduce the proposed edge-aware depth fusion module (grey block in Figure 2).

The original point clouds P are projected to multi-view depth maps, represented as $D = d_{ij} | i = 1, \dots, N_H; j = 1, \dots, N_W \in \mathbb{R}^{N_v \times N_H \times H_W}$, where N_v represents the number of views, N_H and N_W represent the length and height of depth maps.

Multi-view depth maps D are divided into blocks of size $k \times k$ along the x-axis and y-axis, where k is the step size. Then, we use the maximum depth value of each block to fill the whole block through the expanding operation, which connects most scenes in the point cloud depth map. Af-

ter the blocking and expanding operation, multi-view depth maps D are transformed into multi-view dense depth maps D' with the same dimensions.

In the next stage, we calculate the gradient of the multi-view dense depth map along the x-axis and y-axis to extract edge-aware 3D geometry information. Considering each axis has two directions, gradients of dense depth map $G = G^1, G^2, G^3, G^4$, where $G^k = g_{i,j}^k, k = 1, 2, 3, 4$. $g_{i,j}^1, g_{i,j}^2, g_{i,j}^3$, and $g_{i,j}^4$ are defined as:

$$\begin{cases} g_{i,j}^1 = d'_{i,j} - d'_{i+k,j}, \\ g_{i,j}^2 = d'_{i,j} - d'_{i-k,j}, \\ g_{i,j}^3 = d'_{i,j} - d'_{i,j+k}, \\ g_{i,j}^4 = d'_{i,j} - d'_{i,j-k}, \end{cases} \quad (1)$$

where $d'_{i,j}$ is the i^{th} column j^{th} row of multi-view dense depth maps D' . $\{g_{i,j}^k\} \in \mathbb{R}^{N_v \times N_H \times H_W}$ represents one direction of the gradient of multi-view dense depth map.

We take gradients of dense depth map $G \in \mathbb{R}^{N_v \times N_H \times H_W \times 4}$ as input to the max pooling operation on the last dimension and normalization operation. Multi-view edge maps $G' \in \mathbb{R}^{N_v \times N_H \times H_W}$ are obtained to represent the edge of different objects. G' is scaled to $[0, 1]$ by normalization operation.

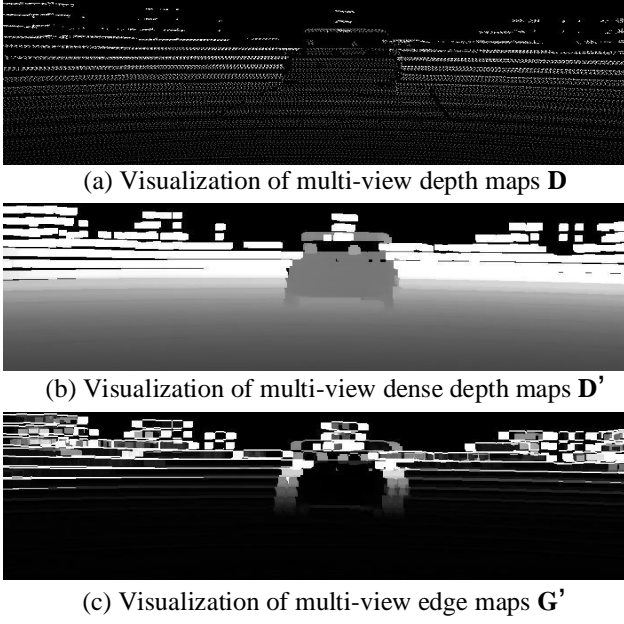


Figure 3. The visualization of (a) multi-view depth maps \mathbf{D} , (b) multi-view dense depth maps \mathbf{D}' , and (c) multi-view edge maps \mathbf{G}' .

As shown in Figure 3 (a), multi-view depth maps \mathbf{D} projected from 3D lidar scanning are sparse, which is not suitable for directly supervising the depth estimation module. Figure 3 (b) shows the multi-view dense depth maps \mathbf{D}' after blocking and expanding operations. Original depth information from depth map is reserved. Main objects in dense depth map are connected, which is beneficial to depth estimation module of the whole scene. In Figure 3 (c), we obtain multi-view edge maps \mathbf{G}' by calculating the maximum gradient value of each pixel along the four directions. The multi-view edge maps \mathbf{G}' represent the maximum depth variation among each block.

After multi-view depth map \mathbf{D} and gradient of multi-view dense depth map \mathbf{G} are obtained, we concatenate \mathbf{D} and \mathbf{G} and feed them to downsampling network to derive the edge-aware 3D features $\mathbf{F}^{ea} \in \mathbb{R}^{N_v \times (N_H/8) \times (N_W/8) \times C_{ea}}$:

$$\mathbf{F}^{ea} = f_{\text{downsample}}(\text{Concat}[\mathbf{D} : \mathbf{G}]), \quad (2)$$

where Concat denotes concatenation operation. $f_{\text{downsample}}$ is the 8x downsampling network consisting of 3 convolutional layers with stride of 1, 4 and 2 respectively. After the downsampling network, \mathbf{F}^{ea} has the same height and weight as 2D camera features \mathbf{V}^{cam} .

3.4. Semantic DepthNet Module

In this section, we introduce the semantic DepthNet module as depicted in Figure 4, which corresponds to the

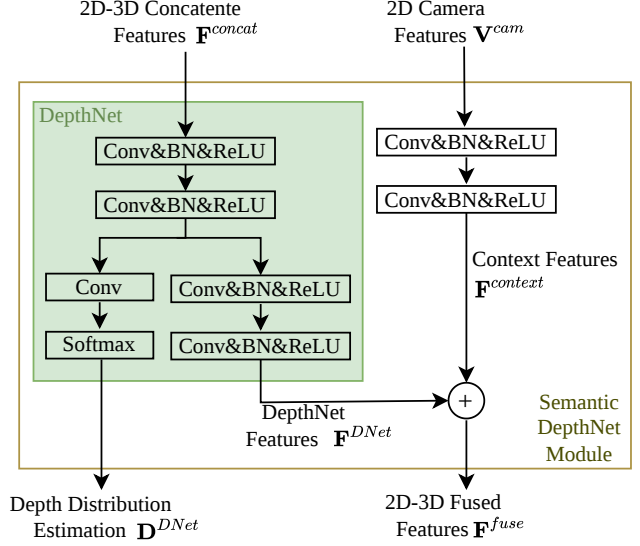


Figure 4. Overview of semantic DepthNet module. Given 2D camera features \mathbf{V}^{cam} and 2D-3D concatenate features \mathbf{F}^{concat} , predicted depth map \mathbf{D}^{DNet} and 2D-3D fused features \mathbf{F}^{fused} are generated by semantic DepthNet module.

yellow block in Figure 2.

As illustrated in Figure 4, the inputs to the semantic DepthNet module are the 2D camera features $\mathbf{V}^{cam} \in \mathbb{R}^{N_v \times (N_H/8) \times (N_W/8) \times C_{cam}}$ and the 2D-3D concatenated features $\mathbf{F}^{concat} \in \mathbb{R}^{N_v \times (N_H/8) \times (N_W/8) \times C_{concat}}$. Given \mathbf{F}^{concat} , depth distribution estimation $\mathbf{D}^{DNet} \in \mathbb{R}^{N_v \times (N_H/8) \times (N_W/8) \times H_D}$, along with its corresponding features $\mathbf{F}^{DNet} \in \mathbb{R}^{N_v \times (N_H/8) \times (N_W/8) \times C_{dnet}}$, are obtained through the DepthNet (green block in Figure 4).

Given \mathbf{V}^{cam} , context features $\mathbf{F}^{context}$ are obtained through two convolutional layers and a skip connection. The fused features \mathbf{F}^{fused} are then acquired through the concatenation operation $\mathbf{F}^{fused} = \text{Concat}[\mathbf{F}^{context} : \mathbf{F}^{DNet}]$. The predicted depth map \mathbf{D}^{DNet} and fused features \mathbf{F}^{fused} serve as the output of the semantic DepthNet module.

3.5. Depth Estimation Module

This section introduces our proposed depth estimation module, which includes sparse depth supervision and gradient edge depth supervision.

The 2D-3D concatenated features \mathbf{F}^{concat} are fed to the depth estimation module (green block in Figure 2) to generate the predicted depth map $\mathbf{D}^{pred} \in \mathbb{R}^{N_v \times N_H \times N_W \times H_D}$. The depth estimation module consists of three deconvolution layers with a stride of two and has the effect of 8x up-sampling.

To supervise the predicted depth map \mathbf{D}^{pred} , multi-view depth maps \mathbf{D} are utilized as ground-truth. Since the multi-view depth maps \mathbf{D} are sparse, we propose sparse depth su-

pervision, where only non-zero pixels in the ground-truth depth map are employed to calculate the loss. As a result, disturbance from zero-valued pixels is effectively eliminated. To concentrate on foreground objects (more objects appear in the background), focal loss is embedded in the sparse depth loss L_{SD} for sparse depth supervision. Sparse depth loss L_{SD} is defined as:

$$L_{SD} = \sum_{i=1}^n \sum_{c=1}^{H_D} -\alpha_c (1 - y_{i,c})^\gamma \log(\hat{y}_{i,c}), \quad (3)$$

where n is the number of non-zero pixels in ground-truth \mathbf{D} . H_D denotes the classes of predicted depth. Here ground-truth \mathbf{D} is transferred to one-hot vectors. $\hat{y}_{i,c}$ is the value of c^{th} class of i^{th} one-hot vector of non-zeros pixels in \mathbf{D} , while $y_{i,c}$ is from the corresponding pixels in predicted depth map \mathbf{D}^{pred} . α_c denotes the weight and γ denotes the predefined hyper-parameter for focal loss.

3.6. Gradient Edge Depth Supervision

Sparse depth supervision accurately utilizes the information from depth maps. However, the sparsity of depth maps affects the accuracy and convergence speed of the depth estimation module. To address this issue, we propose gradient edge depth supervision to focus on the edges of each object. This method uses multi-view dense depth maps \mathbf{D}' as ground truth and multi-view edge maps \mathbf{G}' as weight to alleviate the "depth jump" problem at object boundaries. The gradient edge depth loss L_{GED} for supervision is defined as:

$$L_{GED} = \sum_{i=1}^m \sum_{c=1}^{H_D} -\alpha_c (1 - p_{i,c})^\gamma \log(\hat{p}_{i,c}) * w_i, \quad (4)$$

where m is the number of pixels in the predicted depth map \mathbf{D}^{pred} . H_D denotes the classes of predicted depth. $p_{i,c}$ denotes the value of the c^{th} class of the i^{th} pixel from the predicted depth map \mathbf{D}^{pred} , $\hat{p}_{i,c}$ is the corresponding pixel in the ground-truth depth map \mathbf{D}' , and w_i is the corresponding pixel value of \mathbf{G}' . α_c denotes the weight, and γ denotes the predefined hyper-parameter for focal loss.

The total loss L_{total} is defined as:

$$L_{total} = L_{SD} + L_{GED} + L_{cls} + L_{box}, \quad (5)$$

where L_{SD} and L_{GED} represent the sparse depth loss and gradient edge depth loss defined in Eqn (3) and Eqn (4), respectively. L_{cls} and L_{box} are the classification loss and bounding box loss in the detection head.

4. Experiments

4.1. Implementation Details (Sparse Depth Supervision)

In our experiments, we use BEVFusion [31]/ BEVFusion [10]/ BEVDepth [25] as the baseline to verify the effectiveness and efficiency of our proposed EA-BEV.

In the blocking and expanding operation of the edge-aware depth reconstruction module, step size k is set to 7. The number of views N_v is set to 6. Height and weight of depth maps N_H and N_W are set to 256 and 704. The number of channels C_{ea} , C_{cam} , C_{dnet} , and $C_{context}$ are set to 64, 256, 128, and 128, respectively. The classes of predicted depth H_D are set to 118. Both L_{SD} and L_{GED} adopt focal loss, and γ and α_c are set to 2.0 and 0.25, respectively. Our training environment is on a server with 8 NVIDIA A100 GPUs and an AMD EPYC 7402 CPU.

4.2. Comparison Results

4.2.1 nuScenes 3D Object Detection

To evaluate the effectiveness of our proposed EA-BEV Projector, we conduct comparison experiments on the nuScenes Dataset. This dataset contains 40k labeled samples, with 23 different classes. We use mean Average Precision (mAP) and nuScenes detection score (NDS) as evaluation indicators. Mean mAP score and mean NDS score of 10 foreground classes on the validation set are reported.

Table 1 reports experiment results of the nuScenes 3D object detection validation dataset. Our proposed EA-BEV projector can be added to any LSS-based baseline methods [25, 31, 10] with negligible increment of inference time. When using BEVDepth-R50 [25] as a baseline, the mAP score and NDS score increase by 5.3% and 0.7% after applying the proposed EA-BEV projector. On the BEVFusion [31] baseline, the mAP score and NDS score increase by 0.9% and 0.4%. On the BEVFusion [10] baseline, the mAP score and NDS score increase by 0.5% and 0.5%.

In Table 2, we report the experiment results of the nuScenes 3D object detection test dataset. On the BEVFusion [10] baseline, the mAP score and NDS score increase by 0.2% and 0.2%.

4.2.2 nuScenes BEV Map Segmentation

To evaluate generalization capability, experiments on nuScenes BEV Map Segmentation (i.e., semantic segmentation) task are conducted. Following the same training strategy of baseline method BEVFusion [31], we report the Intersection-over-Union (IoU) score of drivable area, pedestrian cross, walkway, stop line, carpark, divider. A single model that jointly performs binary segmentation for all classes, instead of following conventional approach, is employed to train a separate model for each class

Method	Modality	Resolution	mAP	NDS	Latency(ms)
BEVFormer [32]	C	900×1600	41.6	51.7	-
CenterPoint [30]	L	-	59.6	66.8	80.7
TransFusion-L [22]	L	-	65.5	70.2	-
FUTR3D [3]	C+L	-	64.5	68.3	321.4
MVP [17]*	C+L	-	66.1	70.0	187.1
PointAugmenting † [19]	C+L	-	66.8	71.0	-
TransFusion [22]	C+L	448×800	67.5	71.3	156.6
DeepInteraction [29]	C+L	640×1600	69.9	72.6	204.1
BEVDepth-R50 [25]	C	256×704	35.1	47.5	110.3
+EA-BEV	C	256×704	40.4	48.2	114.8
BEVFusion [31]	C+L	256×704	68.5	71.4	119.2
+EA-BEV	C+L	256×704	69.4	71.8	123.6
BEVFusion [10]	C+L	448×800	69.6	72.1	190.3
+EA-BEV	C+L	448×800	70.3	72.6	194.9

Table 1. Comparison results of 3D object detection on nuScenes validation dataset. † means using TTA(test-time augmentation), * is reported from [31]. After using our proposed EA-BEV projector, mAP scores of LLS-based baseline methods BEVDepth-R50 [25], BEVFusion [31] and BEVFusion [10] increase 5.3%, 0.9% and 0.5%, respectively. While the increment of inference time is only less than 5%.

Method	Modality	mAP ↑	NDS ↑	mATE ↓	mASE ↓	MAOE ↓	mAVE ↓	mAAE ↓
BEVDet [7]	C	42.2†	48.2†	0.529	0.236	0.396	0.979	0.152
BEVFormer [32]	C	44.5	53.5	0.582	0.256	0.375	0.378	0.126
BEVDet4D [6]	C	45.1†	56.9†	0.511	0.241	0.386	0.301	0.121
Pointpillars [5]	L	30.5	45.3	0.517	0.290	0.500	0.316	0.368
SECOND [27]	L	52.8	63.3	-	-	-	-	-
CenterPoint [16]	L	60.3	67.3	0.262	0.239	0.361	0.288	0.136
PointAugmenting [19]	C+L	66.8 †	71.0 †	0.253	0.235	0.354	0.266	0.123
MVP [17]	C+L	66.4	70.5	0.263	0.238	0.321	0.313	0.134
TransFusion [22]	C+L	68.9	71.6	0.259	0.243	0.359	0.288	0.127
CMT [9]	C+L	70.4	73.0	0.299	0.241	0.323	0.240	0.112
DeepInteraction-base [29]	C+L	70.8	73.4	0.257	0.240	0.325	0.245	0.128
BEVFusion [10]	C+L	71.3	73.3	0.250	0.240	0.359	0.254	0.132
+EA-BEV	C+L	71.8	73.6	0.249	0.237	0.342	0.269	0.132

Table 2. Comparison results of 3D object detection on nuScenes test dataset. † means using TTA.

In Table 3, we report comparison results of BEV map segmentation task on nuScenes validation Dataset. After adding the proposed EA-BEV projector to baseline method BEVFusion [31], the mean IoU score increase 0.4 %, which demonstrates generalization capability.

4.3. Ablation Study

4.4. Ablation Study

To examine the effectiveness of each component, we provide an ablation study in Table 4. We use BEVFusion [31] as the baseline method. C means adding context features $F^{context}$ in the semantic DepthNet module; DEN represents the depth estimation module; SDL represents the sparse depth loss; CONCAT-G represents concatenating the gradient of multi-view dense depth map G in the edge-aware

depth fusion module; EGD represents the edge gradient depth loss. Increased mAP scores and NDS scores in Table 4 demonstrate the effectiveness of the mentioned components.

Table 5 provides performances on the nuScenes 3D object detection validation dataset when using different step sizes k of the blocking and expanding operation in the edge-aware depth fusion module. We use BEVFusion [31] as the baseline method. The best mAP score and NDS score are achieved when $k = 7$.

4.5. Qualitative Evaluation

We provide visualization results (Figure 5 and Figure 6) to demonstrate the effectiveness of our proposed EA-BEV projector on nuScenes BEV map segmentation

Method	Modality	Drivable	Ped.Cross.	Walkway	Stop Line	Carpark	Divider	Mean
OFT [13]	C	74.0	35.3	45.9	27.5	35.9	33.9	42.1
LSS [8]	C	75.4	38.8	46.3	30.3	39.1	36.5	44.4
CVT [33]	C	74.3	36.8	39.9	25.8	35.0	29.4	40.2
PointPillars [5]	L	72.0	43.1	53.1	29.7	27.7	37.5	43.8
CenterPoint [16]	L	75.6	48.4	57.5	36.5	31.7	41.9	48.6
PointPainting [18]	C+L	75.9	48.5	57.1	36.9	34.5	41.9	49.1
MVP [17]	C+L	76.1	48.7	57.0	36.9	33.0	42.2	49.0
BEVFusion [31]	C+L	85.5	60.5	67.6	52.0	57.0	53.7	62.7
+EA-BEV	C+L	85.8	61.1	68.0	52.3	56.8	54.5	63.1

Table 3. Comparison results of BEV map segmentation task on nuScenes validation Dataset. We report the IoU score of drivable area, pedestrian cross, walkway, stop line, carpark, divider and the mean IoU score. The mean IoU score increases 0.4 % after adding our proposed EA-BEV projector to the baseline method BEVFusion [31].

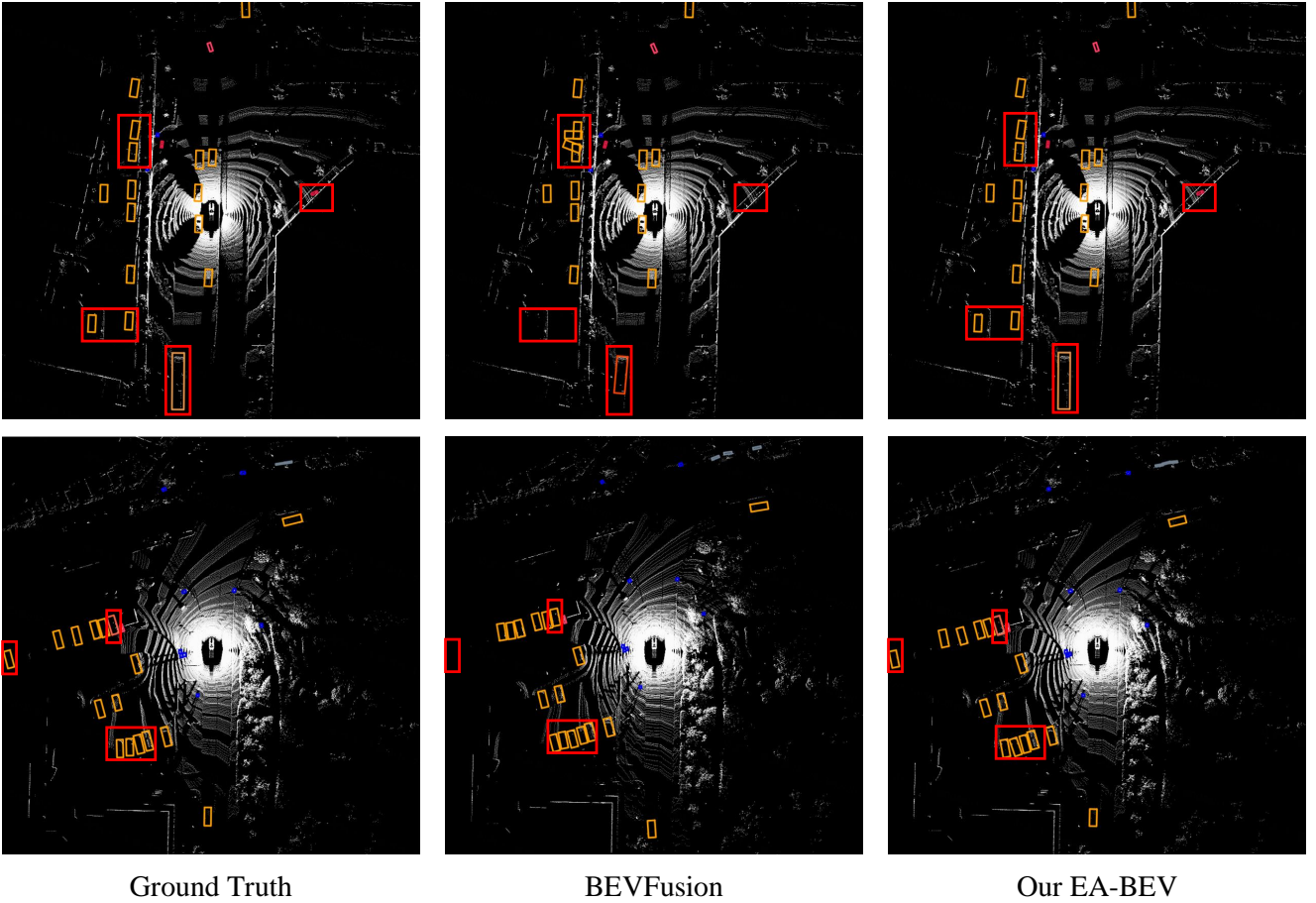


Figure 5. Visualization of the nuScenes 3D object detection validation dataset. From the left to the right, we provide results of ground-truth, baseline method BEVFusion [31] before and after adding our proposed EA-BEV projector. We can observe that results after adding our proposed EA-BEV projector are better than before.

and nuScenes 3D object detection. We show the visualization results of the nuScenes 3D object detection validation dataset in Figure 5. We provide the experiment results of ground-truth, baseline method BEVFusion [31], and baseline method with our proposed EA-BEV projector in the

first column, second column, and third column. The cars are shown in yellow, pedestrians are shown in blue, and trucks are shown in pink. We can capture more target objects by adding our proposed EA-BEV projector than using the baseline method BEVFusion [31] only.

C	DEN	SDL	CONCAT-G	EGDL	mAP	NDS
×	×	×	×	×	68.5	71.4
✓	×	×	×	×	68.6	71.5
✓	✓	✓	×	×	68.7	71.6
✓	✓	✓	✓	×	69.1	71.7
✓	✓	✓	✓	✓	69.4	71.8

Table 4. Ablation study of 3D object detection on nuScene validation dataset. C: context feature $F^{context}$ in semantic DepthNet module, DEN: depth estimation module, SDL: sparse depth loss, CONCAT-G: concatenate gradient of multi-view dense depth map G in edge-aware depth fusion module, EGDL: edge gradient depth loss.

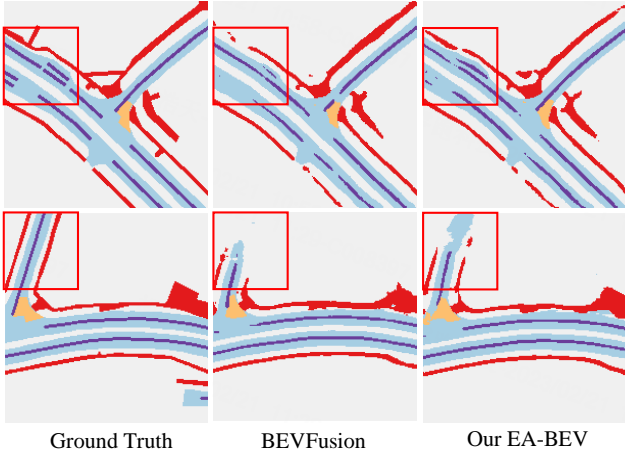


Figure 6. Visualization of the nuScenes BEV map segmentation validation dataset. From the left to the right, we provide results of ground-truth, baseline method BEVFusion [31] before and after adding EA-BEV projector.

k	mAP	NDS
3	68.9	71.6
5	69.1	71.6
7	69.4	71.8
9	68.4	71.4

Table 5. Performances on nuScenes 3D object detection validation dataset when using different step k of blocking and expanding operation in edge-aware depth fusion module.

In Figure 6, we provide the qualitative evaluation on the nuScenes BEV map segmentation validation dataset. From left to right, we provide the results of ground-truth, baseline method BEVFusion [31], and baseline method with our proposed EA-BEV projector. The drivable areas are shown in blue, the lane dividers are shown in purple, the walkways are shown in red, and the crosswalks are shown in pink. From the red bounding boxes, we can observe that the results of adding our proposed EA-BEV projector are better than using the baseline method only.

5. Conclusion

This paper proposes the EA-BEV projector to alleviate the "depth jump" problem and better utilize depth information to supervise depth prediction tasks on 3D outdoor object detection. Our proposed EA-BEV projector is plug-and-play and can be used in any LSS-based methods. Moreover, we propose an edge-aware depth fusion module and gradient edge depth supervision, as well as a depth estimation module to generate estimated depth distribution more accurately. To validate effectiveness and efficiency, we conduct experiments on nuScenes 3D object detection benchmarks and BEV map segmentation benchmarks. It is expected that our proposed EA-BEV projector can inspire further research on depth estimation of 3D outdoor object detection.

References

- [1] Lu C., Molengraft van de M. J. G., and Dubbelman G. Monocular semantic occupancy grid mapping with convolutional variational encoder-decoder networks. *IEEE Robotics and Automation Letters*, pages 445–452, 2019. 2
- [2] Reading C., Harakeh A., Chae J., and Waslander S. L. Categorical depth distribution network for monocular 3d object detection. In *Proceedings of the IEEE/CVF Conference on Computer Vision and Pattern Recognition*, pages 8555–8564, 2021. 2, 3
- [3] Xuanyao Chen, Tianyuan Zhang, Yue Wang, Yilun Wang, and Hang Zhao. Futr3d: A unified sensor fusion framework for 3d detection. *arXiv preprint arXiv:2203.10642*, 2022. 7
- [4] Caesar H., Bankiti V., Lang A. H., Vora S., Liong V. E., Xu Q., Krishnan A., Pan Y., Baldan G., and Beijbom O. nuscenes: A multimodal dataset for autonomous driving. In *CVPR*, 2020. 2
- [5] Lang A. H., Vora S., Caesar H., Zhou L., Yang J., and Beijbom O. Pointpillars: Fast encoders for object detection from point clouds. In *IEEE Conference on Computer Vision and Pattern Recognition*, 2019. 7, 8
- [6] Huang J. and Huang G. Bevdet4d: Exploit temporal cues in multi-camera 3d object detection. *arXiv preprint arXiv:2203.17054*, 2022. 7
- [7] Huang J., Huang G., Zhu Z., and Du D. Bevdet: High-performance multi-camera 3d object detection in bird-eye-view. *arXiv preprint arXiv:2112.11790*, 2021. 1, 2, 3, 7
- [8] Philion J. and Fidler S. Lift, splat, shoot: Encoding images from arbitrary camera rigs by implicitly unprojecting to 3d. In *European Conference on Computer Vision*, pages 194–210, 2020. 1, 4, 8
- [9] Yan Junjie, Liu Yingfei, Sun Jianjian, Jia Fan, Li Shuailin, Wang Tiancai, and Zhang Xiangyu. Cross modal transformer via coordinates encoding for 3d object detection. *arXiv preprint arXiv:2301.01283*, 2023. 7
- [10] Tingting Liang, Hongwei Xie, Kaicheng Yu, Zhongyu Xia, Zhiwei Lin, Yongtao Wang, Tao Tang, Bing Wang, and Zhi Tang. Bevfusion: A simple and robust lidar-camera fusion framework. In *Neural Information Processing Systems (NeurIPS)*, 2022. 2, 6, 7

- [11] Ze Liu, Yutong Lin, Yue Cao, Han Hu, Yixuan Wei, Zheng Zhang, Stephen Lin, and Baining Guo. Swin transformer: Hierarchical vision transformer using shifted windows. In *Proceedings of the IEEE/CVF international conference on computer vision*, pages 10012–10022, 2021. 3
- [12] Li Q., Wang Y., Wang Y., and Zhao H. Hdmapnet: An online hd map construction and evaluation framework. *arXiv preprint arXiv:2107.06307*, 2021. 2
- [13] Thomas Roddick, Alex Kendall, and Roberto Cipolla. Orthographic feature transform for monocular 3d object detection. In *In BMVC*, 2019. 8
- [14] Chen S., Wang X., Cheng T., Zhang Q., Huang C., and Liu W. Polar parametrization for vision-based surround-view 3d detection. *arXiv preprint arXiv:2206.10965*, 2022. 3
- [15] Wang T., Lian Q., Zhu C., Zhu X., and Zhang W. Mv-fcos3d++: Multi-view camera-only 4d object detection with pretrained monocular backbones. *arXiv preprint arXiv:2207.12716*, 2022. 2, 3
- [16] Yin T., Zhou X., and Krähenbühl Philipp. Center-based 3d object detection and tracking. In *CVPR*, 2021. 7, 8
- [17] Yin T., Zhou X., and Krähenbühl Philipp. Multimodal virtual point3d detection. *M. Ranzato, A. Beygelzimer, Y. N. Dauphin, P. Liang and J.W. Vaughan, Eds.*, pages 16494–16507, 2021. 7, 8
- [18] Sourabh Vora, Alex H Lang, Bassam Helou, and Oscar Beijbom. Pointpainting: sequential fusion for 3d object detection. In *In CVPR*, 2020. 8
- [19] Chunwei Wang, Chao Ma, Ming Zhu, and Xiaokang Yang. Pointaugmenting: Cross-modal augmentation for 3d object detection. In *Proceedings of the IEEE/CVF Conference on Computer Vision and Pattern Recognition*, pages 11794–11803, 2021. 7
- [20] T. Wang, X. Zhu, J. Pang, and D. Lin. Fcos3d: Fully convolutional one-stage monocular 3d object detection. *arXiv preprint arXiv:2104.10956*, 2021. 2
- [21] Xiaopei Wu, Liang Peng, Honghui Yang, Liang Xie, Chenxi Huang, Chengqi Deng, Haifeng Liu, and Deng Cai. Sparse fuse dense: Towards high quality 3d detection with depth completion. *arXiv preprint arXiv:2203.09780*, 2022. 2, 3
- [22] Bai X., Hu Z., Zhu X., Huang Q., Chen Y., Fu H., and Tai C. Transfusion: Robust lidar-camera fusion for 3d object detection with transformers. In *CoRR*, 2022. 7
- [23] Zhou Xingyi, Wang Dequan, and Krähenbühl Philipp. Objects as points. *arXiv preprint arXiv:1904.07850*, 2019. 2
- [24] Liu Y., Yan J., Jia F., Li S., Gao Q., Wang T., Zhang X., and Sun J. Petrv2: A unified framework for 3d perception from multi-camera images. *arXiv preprint arXiv:2206.01256*, 2022. 2, 3
- [25] Li Y., Ge Z., Yu G., Yang J., Wang Z., Shi Y., Sun J., and Li Z. Bevdepth: Acquisition of reliable depth for multi-view 3d object detection. *arXiv preprint arXiv:2206.10092*, 2022. 1, 2, 6, 7
- [26] Wang Y., Guizilini V. C., Zhang T., Wang Y., Zhao H., and Solomon J. Detrv3d: 3d object detection from multi-view images via 3d-to-2d queries,” in conference on robot learning. In *PMLR*, pages 180–191, 2022. 2, 3
- [27] Yan Y., Mao Y., and Li B. Second: Sparsely embedded convolutional detection. In *Sensors*, 2018. 3, 7
- [28] You Y., Wang Y., Chao W.-L., Garg D., Pleiss G., Hariharan B., Campbell M., and Weinberger K. Q. Pseudo-lidar++: Accurate depth for 3d object detection in autonomous driving. In *in ICLR*, 2020. 2, 3
- [29] Zeyu Yang, Jiaqi Chen, Zhenwei Miao, Wei Li, Xiatian Zhu, and Li Zhang. Deepinteraction: 3d object detection via modality interaction. In *NeurIPS*, 2022. 7
- [30] Tianwei Yin, Zhou Xingyi, and Philipp Krahenbuhl. Centerbased 3d object detection and tracking. In *Proceedings of the IEEE/CVF Conference on Computer Vision and Pattern Recognition*, pages 11784–11793, 2021. 7
- [31] Liu Z., Tang H., Amini A., Yang X., Mao H., Rus D., and Han S. Bevfusion: Multi-task multi-sensor fusion with unified bird’s-eye view representation. In *CoRR*, 2022. 1, 2, 6, 7, 8, 9
- [32] Li Z., Wang W., Li H., Xie E., Sima C., Lu T., Qiao Y., and Dai J. Bevformer: Learning bird’s-eye-view representation from multicamera images via spatiotemporal transformers. *arXiv preprint arXiv:2203.17270*, 2022. 2, 3, 7
- [33] Bardy Zhou and Philipp Krähenbühl. Cross-view tranformer for real-time map-view semantic segmentation. In *In CVPR*, 2022. 8